Sensors & Transducers Journal, Vol. 137, Issue 2, February 2012, pp. 155-164

www.sensorsportal.com

Sensors & Transducers

ISSN 1726-5479

http://www.sensorsportal.com

Nanocrystalline Tin Oxide to be Applied in a Gas Sensor

[1] Mario F. BIANCHETTI, [2] Ines BRACKO, [2] Sreco Davor SKAPIN, [1] Noemí E. WALSÖE de RECA

[1] CINSO (Centro de Investigaciones en Sólidos) CONICET-CITEDEF,
Juan B. de La Salle 4397, Villa Martelli (B1603ALO) Buenos Aires, Argentina
[2]Advanced Materials Department, Jožef Stefan Institute, Jamova 39,
1000 Ljubljana, Slovenia

Received: 24 November 2011 /Accepted: 14 February 2012 /Published: 28 February 2012

Abstract: The aim of this paper was to describe the methods of nanocrystalline SnO_2 preparation and to show the improvement of the behaviour of a hydrogen sensor built with the grown SnO_2 nanoparticles since particular properties of the nanomaterial are related to the sensor response. Nanocrystalline SnO_2 was synthesized by gel-combustion and by reactive oxidation methods. Characterization was performed by X-Ray Diffraction (XRD), Brunauer-Emmer-Teller isotherms (BET) absorption and by High Resolution Transmission Electron Microscopy (HRTEM). A careful characterization enabled to control the crystallites size and properties to improve the behaviour of a hydrogen sensor. It was proved that if nanocrystalline SnO_2 was used to build the resistive sensor, replacing the conventional microcrystalline SnO_2, the sensor sensitivity increased between 30 and 35 % (according to the grown crystallites size of nanocrystalline SnO_2) and the working temperature (T_w) decreased from 350-450 ºC to 180-220 ºC. The T_w decrease obliged to improve the heating and measuring system of sensor which is also described. *Copyright © 2012 IFSA.*

Keywords: Nanocrystalline tin oxide, Synthesis and characterization of tin oxide, Gel-combustion, Reactive oxidation method, Hydrogen sensor.

1. Introduction

Tin dioxide has been studied for a long time because it exhibits interesting properties considerably changing as the SnO_2 grain size decreases to nanometric dimensions.

Some authors of this work have already used this material to build resistive gas sensors, i.e. for VOCs, CO or H_2 [1-6] and if nanocrystalline SnO_2 was used to build sensors for hydrogen, replacing the conventional microcrystalline SnO_2, amazing results have been found. Consequently, the study of structural and morphological properties of nanocrystalline SnO_2 results important to understand the sensing mechanisms and to improve the sensors performance. The gas detection process is affected by several factors, among them the microstructure of the sensing material since gas sensing is produced by the change of the surface electrical resistance. The metallic oxide semiconductor previously reacts with the oxygen of air forming, at the semiconductor surface, oxygen adsorbates, such as O^-, O_2^-, O^{2-} [7, 8]. These adsorbates (being the O^- the most active) play an important role in gas sensing covering the semiconductor surface and grain boundaries and reacting, at a working temperature (T_w) ~ 350-450 ^oC if the sensor is built with the microcrystalline semiconductor. In case of *n*-type semiconductor metallic oxides, the formation of these adsorbates builds a space-charge region, resulting in an electron-depleted surface layer (space-charge) due to the electron transfer to the adsorbates as follows:

$$O_2(g) + 2e^- = 2O^- \text{ (adsorb.)} \quad (1)$$

The depth of the space-charge is a function of the surface coverage with the oxygen adsorbates and of the intrinsic electron concentration in the bulk. The resistance of the *n*-semiconductor is, in consequence high, because a potential barrier to the electronic conduction is formed at each grain boundary [9]**.** If the sensor is exposed to a reducing gas (i.e. H_2) at the T_w, the gas reacts with oxygen adsorbate according to:

$$H_2 + O^- = H_2O + e^- \quad (2)$$

The oxygen adsorbates are consumed by the subsequent reactions, so that a lower steady-state is established, the potential barrier height decreases and a drop in resistance are produced. The resistance variation is the measuring parameter of the semiconductor gas sensor [7].

Sensor sensitivity (S) can be defined as:

$$S = R_{air} / R_{air + gas}\ , \quad (3)$$

where: R_{air} is the resistance in air and $R_{air + gas}$ is the resistance in a gas sample containing a reducing component. The reactivity of the oxygen adsorbates is a function of the kind of reducing gas and of sensor temperature.

A simple schematic but interesting model for grain-size effects on the surface resistivity was proposed by Yamazoe et al. [7] concluding that sensor sensitivity increases as grain size decreases.

The aim of this work was to study the structure and morphology of nanocrystalline SnO_2 (with different crystallite sizes) used to build a hydrogen sensor analyzing the device performance related to the nanoparticles properties. Nanocrystalline SnO_2 was prepared by gel-combustion and by a reactive oxidation with H_2O_2 method and characterized by X-Ray Diffraction (XRD) to identify the material, to evaluate the crystalline structure and to measure crystallites size; by Brunauer-Emmer-Teller isotherms

(BET) to determine the specific area and by High Resolution Transmission Electron Microscopy (HRTEM) to study the morphology and size distribution of crystallites.

2. Experimental Procedure

2.1. SnO_2 Properties and Preparation

SnO_2 exhibits a tetragonal crystalline structure, being its mineral form called cassiterite with space group: D_{4h}^{14} (or $P4_2/mnm$) exhibiting two metal atoms and four oxygen atoms in the unit cell. Each metal atom is surrounded by six oxygen atoms nearly forming the corners of a regular octahedron. Oxygen atoms are surrounded by three tin atoms nearly situated at the corners of an equilateral triangle. The lattice parameters are a = b = 4.737Å and c = 3.186Å.

Nanocrystalline SnO_2 has been prepared by two techniques: A) gel-combustion and B) by reactive oxidation with H_2O_2 [5, 10-11]. The gel combustion method (A) is based on the preparation of nanocrystalline SnO_2 powder by means of a nitrate-citrate gel-combustion method starting from metallic tin [11]. Gel-combustion methods are based on the rapid ignition of a gel formed by a salt of the desired metal (i.e. nitrates, which are strong oxidizers) and an organic fuel: citric acid [6, 12-14]. The precursor is an aqueous solution of pure metallic Sn (Mallincrodt), nitric acid (70 %, Merck), citric acid (Merck) and ammonium hydroxide (25 %, Merck) which is prepared with a [tin/fuel] ratio of 1:6. The pH of solution was adjusted to 7. The solution is concentrated by heating to ~(80-90) ºC in a Pyrex vessel under constant stirring and a slow concentration is followed without producing any precipitation until it turns into a viscous gel. The reaction between the nitrate ion and the organic fuel is strongly exothermic. The large volume of gases produced during combustion disintegrates the precursor gel, being this process followed by calcination, which eliminates the organic residues, yielding small crystallites with nanometric size: (9-15) nm. Parameters to be adjusted are, among others, the type of organic fuel, temperature and duration of combustion, the crystallites size and homogeneity, their morphology and the impurities retention during the synthesis process, among others. The election of the [tin/fuel] ratio and the ignition conditions and calcination temperature were discussed in detail in [10].

The reactive oxidation method (B) is simpler than A to be applied. It consists in treating the $SnCl_2$ with H_2O_2 and the resulting product with $(NH_4)OH$ in H_2O_2 medium, producing stannic acid which gives SnO_2 by calcination [15]:

$$SnCl_2 + H_2O_2 \rightarrow SnOCl_2 + H_2O$$

$$SnOCl_2 + 2(NH_4)\,OH \xrightarrow{H_2O_2} SnO_3H_2 + 2\,(NH_4)Cl \quad (4)$$

$$\downarrow$$

calcination: SnO_2

The strongly oxidation with H_2O_2 yields small crystallites with nanometric size (2-9 nm).

2.2. Characterization Techniques

X-Ray Diffraction (XRD) patterns of nanocrystalline powders are performed in a Philips PW 3710 diffractometer using the Cu $K\alpha_1$ radiation with the pure cassiterite spectrum as reference. In nanomaterials, the XRD *peak broadening* with decreasing particle size, is a well known phenomenon [16] and it can be used to determine the particle size, s, by the Scherrer equation:

$$s = k \lambda / \beta \cos \theta, \quad (5)$$

where: k is a constant (usually taken as 0.89), λ is the wavelength of the X-ray beam, β is the full width at half maximum height (FWHM) of a given peak (after removal of the instrumental broadening) and θ is the diffracted angle of the peak. Scherrer equation represents the simplest treatment of peak broadening and it can be extended to include the effect of strain broadening of the peaks [17]. Clearly, this method will only yield an average particle size (in many cases depending on the synthesis conditions) and it will not provide information on the dispersion of size or the extent of grains agglomeration.

Specific surface area (m^2/g) of calcined powders is measured by *Brunauer-Emmet-Teller (BET) isotherm technique* with nitrogen absorption on the surface as performed with an Autoabsorb-1 Quantachrome Instrument. The average particle size (d) is calculated by:

$$d = 6/ \rho A,$$

where: ρ is the theoretical density of material (in this case: 6.95 $g.cm^{-3}$) and A is the specific surface area of the powder. *High Resolution Transmission Electron Microscopy (HRTEM)* is used to study morphological characteristics of nanostructures, with a JEM-2100-JEOL microscope and with a Philips PW6061 CM200, PW 6595/55 microscope.

2.3. Hydrogen Sensor

Resistive hydrogen sensors were built with the nanocrystalline semiconductor SnO_2, detecting 5 ppm H_2 in air [1]. Pure nanocrystalline SnO_2, as synthesized with the methods and characterized with techniques described in the paragraph 2.2., was deposited at first on AlSiMg substrates and, afterwards, because of the T_w decrease, on ($Si + N_xSi_y$).

3. Results and Discussion

3.1. Nanocrystalline SnO_2

It is important to point out that all the characterization techniques data, were completely in agreement among them if characterization was performed on nanocrystalline SnO_2 exhibiting the same crystallite size, no matter which of the two methods (A or B) were used to synthesize the powders. To reduce this paper length, only results from the second synthesis method are considered here. Results of nanocrystalline SnO_2 specimen are reported in Table 1: crystallite size (nm), calcination temperature (ºC) and BET data ($m^2.g^{-1}$). All the XRD analyzed samples exhibit the cassiterite SnO_2 tetragonal rutile structure. Fig. 1 shows the superimposed spectra of two specimen of Table 1: specimen 1 calcined at 440 ºC (thick line) and specimen 7 calcined a 1600 ºC (thin line). Cassiterite diffraction lines appear in all the patterns with the *(hkl)*: (110), (101), (200), (111), (211), (220), (002), (310), (112) and (301). Differences of both spectra of Fig. 1 are assigned to the different crystallite sizes (since the broadening of peaks due to the smaller crystallite size is clearly observed) being this fact also related to the calcination temperature.

BET adsorption measurements showed higher specific area values for the smallest particles size. In Fig. 2, BET specific area data (in triangles) and grain size (in squares) were plotted versus the calcination temperature, showing the decrease of specific area with the increasing calcination temperature and the grain size variation for the same calcination temperature range.

Table 1. Crystallite size, calcination temperature and BET data of SnO_2 nanoparticles.

Specimen	Crystallite size (nm)	Calcination temperature (ºC)	BET data (m^2/g)
0	(3.7 ± 0,2)	390	--
1	(5,7 ± 0,3)	440	53,3
2	(8,0 ± 0,5)	500	36,5
3	(17,0 ± 1)	600	18,6
4	(26,0 ± 2)	700	14,2
5	(36,0 ± 3)	800	9,90
6	(100,0 ± 20)	1100	7,7
7	> 150,0	1600	

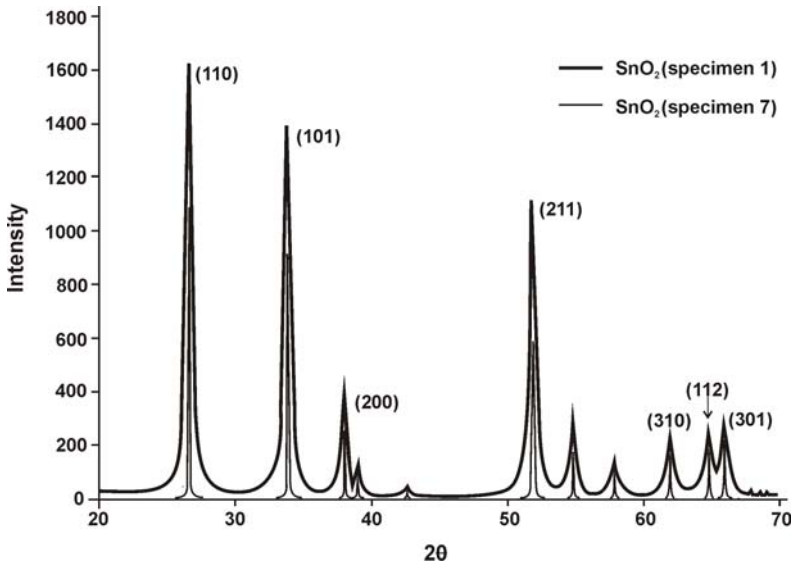

Fig. 1. XRD spectra of the cassiterite structure corresponding to the specimen 7 calcinated at 1600 ºC (thin line, sharp peaks) and to the specimen 1, calcinated a 440 ºC (thick line, broadening of peaks).

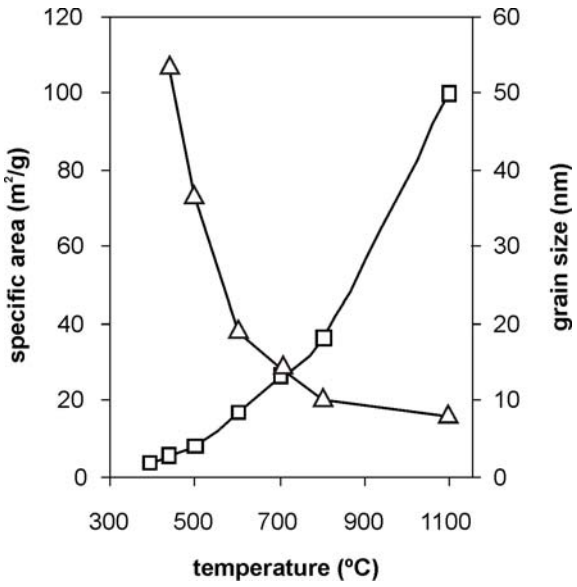

Fig. 2. BET data-specific area ($m^2.g^{-1}$) vs. calcination temperature (ºC) in triangles and grain size (nm) vs. calcination temperature (ºC) in squares.

HRTEM observations enabled to conclude that the increasing calcination temperature produced the change of crystallites size, the size distribution and crystallites shape. Fig. 3. shows the electron diffraction pattern of small sized particles. The diffraction rings were identified verifying that they were in agreement with the spacing of the five planes [(110), (101), (200), (210) and (211)] associated to the cassiterite tetragonal rutile structure, being these planes also identified in the XRD spectra of Fig. 1.

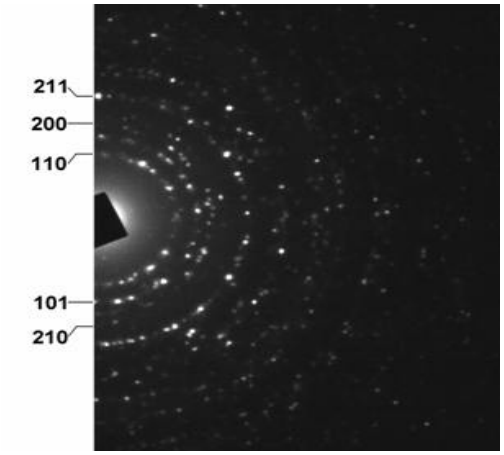

Fig. 3. Electron diffraction pattern of SnO_2 particles.

The SnO_2 nanoparticles morphology was studied with HRTEM. Fig. 4a. is a micrograph of SnO_2, the calcination temperature was 440 ºC and particles exhibited a homogeneous distribution of size, being the mean size value: (5.7 ± 3) nm. Most particles with the smallest grain size, exhibited rounded borders and a high defects density. In Fig. 4b, a particle of Fig. 4a. is observed with higher magnification by HRTEM and defects: stacking faults, twins (CTB coherent twin boundaries) are shown by arrows and dislocations are shown inside the circle (D). Fig. 5a. is the HRTEM micrograph of particles resulting from calcination temperature: 700 ºC and a mean particle size: (26 ± 10) nm was evaluated. Fig. 5b is a magnification of the central particle (circle) of Fig. 5a in which few defects have been observed. Grains are more faceted than those of Fig. 5a. and they do not exhibit so many defects. It is possible that at lower calcination temperature, all the grains exhibit similar defects density and, at higher temperatures and during the grain growth, some defects can move enough to be annihilated in surfaces and drains. At this calcination temperature the crystallites size distribution is not homogeneous as for specimen calcined at lower temperatures.

3.2. Sensor

The resistivity and the working temperature of sensors built with microcrystalline and nanocrystalline materials were measured comparatively. Reference sensors were built with microcrystalline SnO_2 (Ø = 1-6 μm) as prepared by conventional calcination method. Nanocrystalline SnO_2 (prepared and characterized as described in paragraphs 2.1 and 2.2.) with crystallite sizes: 6 nm and 40 nm, was used to build sensors. At first, the nanocrystalline material SnO_2 was deposited (as in case of microcrystalline material) on the top face of an electronic purity AlSiMg substrate (provided with two interdigitated Pt electrodes previously deposited by screen printing). Sensitivity ($S = R_{air} / R_{air + gas}$) of sensors built with nanomaterials resulted from 30 to 35 % higher in comparison with that of reference sensors. The highest value was related to the smallest crystallite size of the nanomaterial. The highest sensitivity was reached at a working temperature (T_w ~ 180-200 ^oC) being interesting to point out that

sensors built with microcrystalline SnO_2 operated in a T_w range of 350-450 ^oC. Fig. 6 is the plot of sensitivity (S) versus the working temperature (T_w in ^oC) of the hydrogen sensor built with nanomaterial.

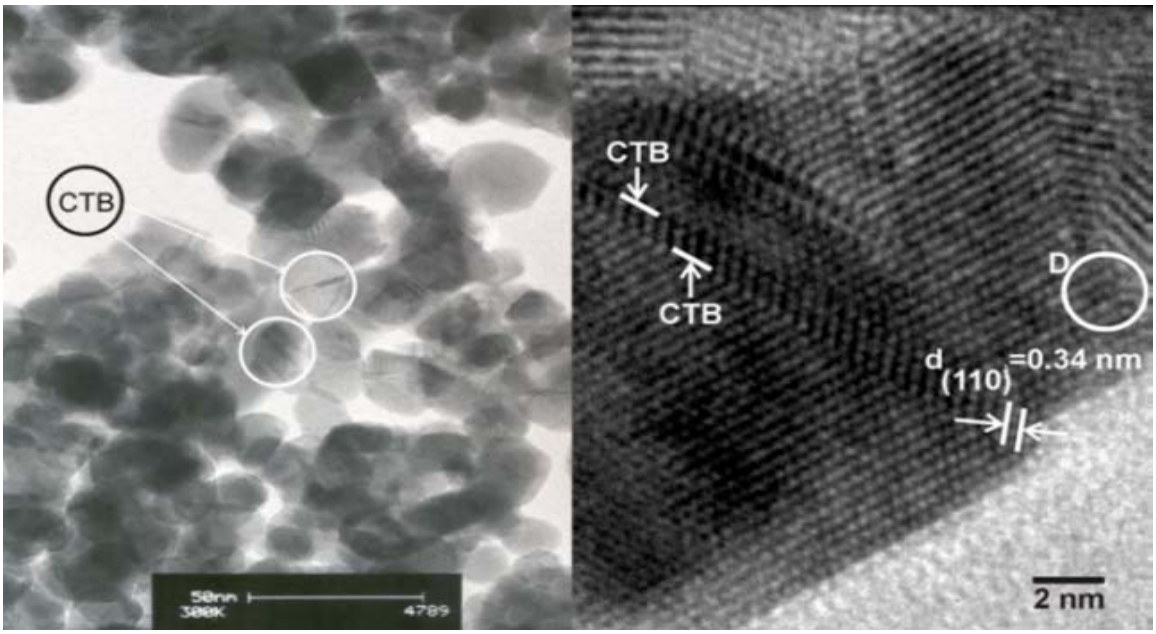

(a) (b)

Fig. 4. (a) HRTEM micrograph of SnO_2 nanoparticles (calcination temperature: 440ºC) Arrows are showing some coherent twin boundaries (CTB); (b) Detail of a particle of Fig. 4a. at higher magnification. Arrows are showing some coherent twin boundaries (CTB) and the circle is around several dislocations (D).

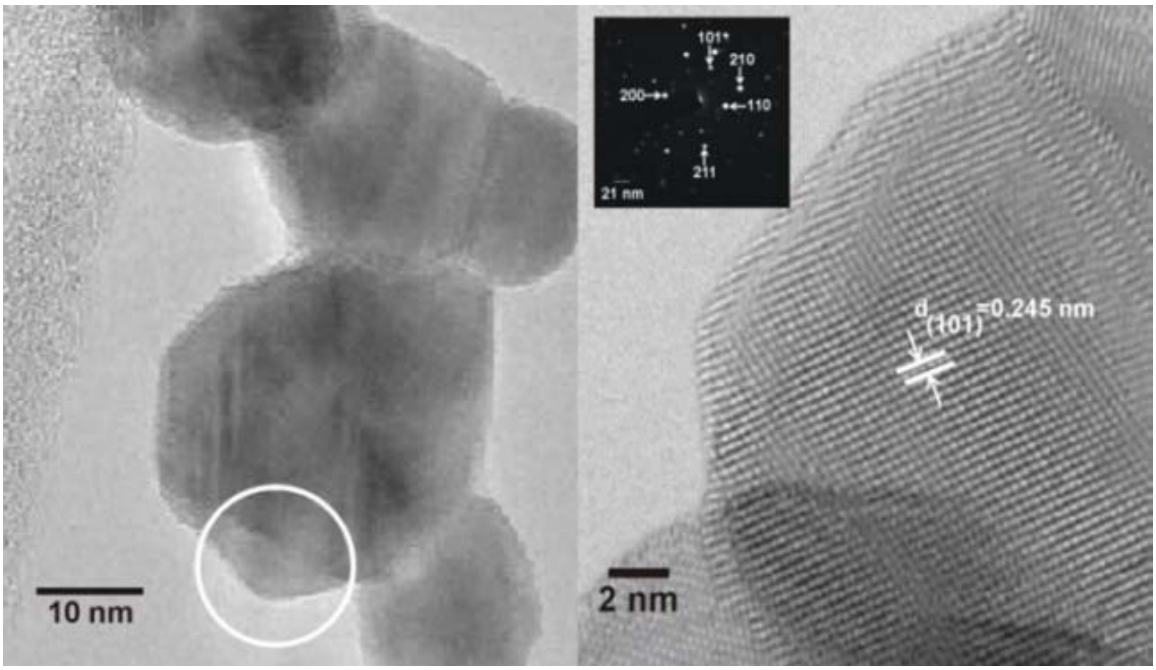

(a) (b)

Fig. 5. (a) HRTEM micrograph of SnO_2 nanoparticles (calcination temperature: 700 ºC) and (b) Detail of a part of the central particle of Fig. 5a. at higher magnification.

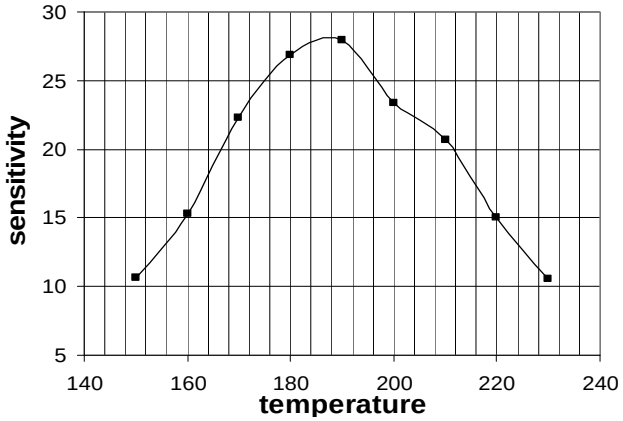

Fig. 6. Sensitivity (S) vs. the working temperature (T_w ^oC).

Due to the lower T_w, in case of using nanocrystalline SnO_2 to build the sensor, an innovative heater and measurement device [2], similar to those used for thin film sensors [18, 19], was developed with MEMS technique to be incorporated to the sensor. It consists of a Si micro-etched substrate (Fig. 7a.), being the micro-machined area obtained by wet-etching of the Si wafer, coated with an N_xSi_x layer to provide a mechanical support (micrograph of Fig. 7b.) On N_xSi_x layer, a Pt film is high vacuum deposited and a double meander structure (heater-contacts system) is built with lift-off technique. This ensemble is provided of a circuit enabling the commutation of the same Pt structure to be used as contact to extract the sensor signal or to act as a heater. The same functional results of conventional heaters for sensors are reached in this case but, using a 10 to 15 times lower energy, making possible to apply sensors to portable equipments.

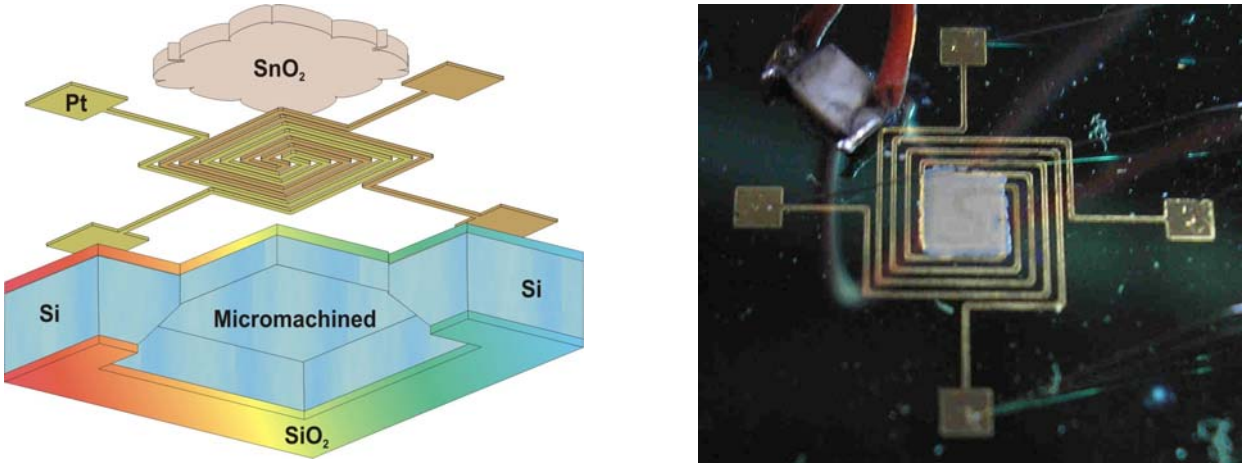

(a) (b)

Fig. 7. (a) Scheme of (Si + N_xSi_y) micromachined structure, and (b) Micrograph of the same area.

In order to use the same Pt structure as heater and contact system to drain the signal, it is necessary to associate an ad-hoc electronic circuit as detailed in Fig. 8.

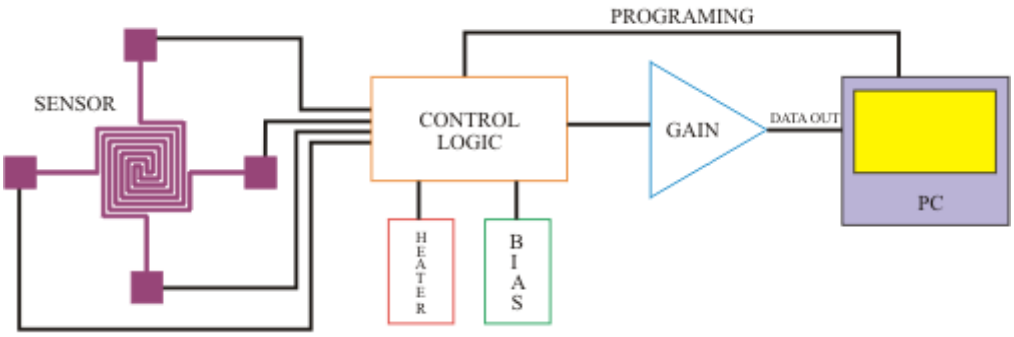

Fig. 8. Commutation system making that electrodes act simultaneously as heater or contacts.

4. Conclusions

SnO_2 nanoparticles with different crystallites size (CS) were prepared by a gel-combustion method (CS: 9-15 nm) and by a reactive oxidation with H_2O_2 method (CS: 2-9 nm). A comparison of both methods data is considered. XRD, BET absorption technique and HRTEM were used to characterize the structural and morphological properties of SnO_2 in order to reach the best characteristics of nanoparticles (with different crystallites size: from 3.7 nm to >150 nm) to be used for resistive gas sensors. The calcination temperature results responsible of the nanoparticles growth and of the specific area decrease. The HRTEM micrographs have shown that rounded nanoparticles with the smallest grain size exhibited a higher defects density and a homogeneous distribution. Particles with larger crystallites size (calcined at higher temperatures) presented faceted grains with considerable lower defects density since faceting is produced by the atoms ability to move and reorganize. Besides, defects in particles calcined at high enough temperatures, can also move to be annihilated in surfaces and drains.

Sensitivity of the hydrogen sensors built with nanomaterial resulted from 30 to 35 % higher in comparison with that of reference sensors, being the highest S value related to the smallest crystallite size. The working temperature decreased to T_w ~ 180-200 ^oC while in case of sensors built with microcrystalline SnO_2 remained T_w ~ 350-450 ^oC. Due to the lower T_w, in case of nanocrystalline SnO_2 sensors, a commutation: heater to measurement device was developed to be incorporated to the sensor saving considerably energy.

Acknowledgements

The authors are indebted to CONICET by the Grant PIP Ner. 1122-00901-00355 (2010/13) and to Eng. Ma. Emilia. F. de Rapp (XRD analysis), Dr. Ismael Fábregas (BET measurements), Eng. H. A. Lacomi (circuits design) and Tech. Fernando Vázquez Rovere (drawings and design) by their valuable assistance.

References

[1]. M. F. Bianchetti, N. E. Walsöe de Reca., A Sensor built with nanocrystalline SnO_2 to detect hydrogen, Application for *A. R. Patent* (in process).

[2]. L. T. Alaniz, C. L. Arrieta, M. F. Bianchetti, C. A. Gillari, J. F. Giménez, H. A. Lacomi, D. F. Valerio and N. E. Walsöe de Reca. A. R., Patent - PP-070105987 on 'Gas sensor with microheating device by direct contact and sensing method', granted on 28/12/2007.

[3]. N. E. Walsöe de Reca, Nanostructured Materials, *Anales Academia Nacional de Ciencias Exactas, Físicas y Naturales*, 59, 2007, pp. 59-93.
[4]. L. B. Fraigi, D. G. Lamas, N. E. Walsöe de Reca, Microsensores de Estado Sólido para Monitoreo de Medio Ambiente, Programa CYTED (Ciencia y Tecnología para el Desarrollo), Proyecto IX. 2, Ed. Control S. R. L., Bs. As., 1999, pp. 57-72.
[5]. L. B. Fraigi. Doctoral Thesis (Engineering), Sensores de CO (g) basados en óxido de estaño nanoestructurado, *FI-Universidad de Buenos Aires*, 2006.
[6]. L. B. Fraigi, D. G. Lamas, N. E. Walsöe de Reca, Novel process to prepare nanocrystalline SnO_2 powders for thick films gas sensors, *Química Analítica* (España), 18, Suppl. 1, 1999, pp. 71.
[7]. N. Yamazoe, J. Fuchigami, M. Kishikawa, T. Seiyama, Interactions of tin oxide surface with O_2, H_2O and H_2, *Surf. Sci*., 86, 1979, pp. 335.
[8]. Yu. A. Dobrovol´skii, G. V. Kalinnikov, Oxygen chemisorption by SnO_2–based oxide electrodes in solid electrolytes, *Élektrokhimiya*, 28, 10, 1992, pp. 1567-1575.
[9]. Y. Shimizu, M. Egashira, Basic aspects and challenges of semiconductor gas sensors, *MRS Bulletin*, 26, 4, 1999, pp. 18.
[10]. L. B. Fraigi, D. G. Lamas, N. E. Walsöe de Reca, Novel method to prepare nanocrystalline SnO_2 powders by a gel-combustion method, *Nanostruct. Mater.*, 11, 1999, pp. 311.
[11]. L. B. Fraigi, D. G. Lamas, N. E. Walsöe de Reca, Comparison between two combustion routes for the synthesis of nanocrystalline SnO_2 powders, *Mater. Lett.*, 47, 2001, pp. 262.
[12]. L. B. Fraigi, R. E. Juárez, D. G. Lamas, G. E. Lascalea, N. E. Walsöe de Reca, Aplicaciones Interdisciplinarias de Materiales, (Ed. J. P. Adrados, J. L. Aragón, M. Torres), *Publish. by de la Torre*, Madrid, Spain, 2002, pp. 7-20.
[13]. M. D. Shaji Kumar, T. M. Srinivasan, P. Ramasamy, C. Subramanian, Synthesis of lanthanum aluminate by a citrate-combustion route, *Mater. Lett*., 25, 1995, pp. 171.
[14]. R. E. Juárez, D. G. Lamas, G. E. Lascalea y N. E. Walsöe de Reca., Synthesis of nanocrystalline Powders of TZP Ceramics by a Nitrate-Citrate Combustion Route, *J. European Ceram. Soc.*, 20, 2000, pp. 133.
[15]. M. F. Bianchetti, N. E. Walsöe de Reca., A novel method to synthesize SnO_2 nanoparticles, Application for *A. R. Patent* (in process).
[16]. H. P. Klug, L. E. Alexander, X-Ray Diffraction Procedures for polycrystalline and amorphous Materials, *Wiley Interscience Publication*, New York, 1974.
[17]. D. Balzar, Defect and Microstructure Analysis from Diffraction, *Oxford University Press*, London, New York, 1999).
[18]. V. Foglietti, A. Bearzotti, P. Degasperis, S. Petrocco, R. Angelucci, G. Cardinali, L. Dori, P. Maccagnini, A. Parisini, A. Poggi, M. Severi, M. Carrozza, P. Dario, B. Magnani, A. Menciassi, Anual Report, Consiglio delle Recherche, *LAMEL*, 1997, pp. 63.
[19]. G. Cardinali, L. Dori, M. Fiorini, I. Sayago, G. Faglia, C. Perego, G. Sverbeglieri, V, Liberati, F. Maloberti, D. Tonietto, Anual Report, Consiglio delle Recherche, *LAMEL*, 1998, pp. 71.
